CrystEngComm

Accepted Manuscript

ROYAL SOCIETY OF CHEMISTRY

www.rsc.org/crystengcomm

Journal Name

RSCPublishing

ARTICLE

Crystal-to-crystal transformations and photoluminescence changes in the Cu(I) coordination networks based on a formamidinate ligand

Cite this: DOI: 10.1039/x0xx00000x

Received 00th January 2012,
Accepted 00th January 2012

DOI: 10.1039/x0xx00000x

www.rsc.org/

Wayne Hsu,[a] Kuan-Ting Chen,[a] Yu-Sian Li,[a] Po-Wen Cheng,[a] Tsun-Ren Chen[b] and Jhy-Der Chen*[a]

One-pot solvothermal reactions of 4-aminopyridine and triethylorthoformate with $Cu(O_2CCH_3)_2$ in acetone (ACT), dimethylformamide (DMF), tetrahydrofuran (THF), methanol (MeOH) and ethanol (EtOH) afforded 2D coordination networks *anti*-{[Cu(4-pyf)]·ACT}$_n$, **1a**, (4-Hpyf = *N,N'*-bis(pyridine-4-yl)formamidine), *anti*-{[Cu(4-pyf)]·DMF}$_n$, **1b**, *anti*-{[Cu(4-pyf)]·THF]}$_n$, **1c**, *syn*-{[Cu_4(4-pyf)$_4$]·2MeOH}$_n$, **2a**, and *syn*-{[Cu_4(4-pyf)$_4$]·2EtOH}$_n$, **2b**, whereas the reaction of $Cu(O_2CCH_3)_2$, 4-aminopyridine, triethylorthoformate and CuX_2 (X = BF_4^- and ClO_4^-) in ethanol gave the 3D coordination networks *syn*-{[Cu_3(4-pyf)$_2$](BF_4)·2H_2O·EtOH}$_n$, **3a** and *syn*-{[Cu_3(4-pyf)$_2$](ClO_4)·EtOH}$_n$, **3b**, respectively, which were characterized by X-ray crystallography. Complexes **1a** – **3b** are the first 2D and 3D coordination networks showing closed-shell Cu(I)---Cu(I) interactions that are supported by the formamidinate ligands. Reversible crystal-to-crystal transformations were observed for the 2D *anti*- and *syn*-coordination networks upon solvent exchange. Irreversible *anti* to *syn* crystal-to-crystal transformations can be shown upon solvent removal and the important intermediate, *syn*-{[Cu_4(4-pyf)$_4$]·2THF}$_n$, **2c**, that verifies the temperature-dependent transformation was structurally characterized. The configurations of the structures have significant influences on the emission properties. While the *syn*-complexes show broad emissions, those of the *anti*-complexes are not detectable, indicating cuprophilicity is unlikely to play significant roles in determining the emissions of **1a** – **3b**. The 2D *anti*- and *syn*-complexes that show outwardly dangling pyridyl rings may adsorb the Cd salts through Cd---N interactions.

Introduction

The design and synthesis of coordination polymers with controlled dimensionality is a rapidly developing field in supramolecular chemistry and crystal engineering.[1] The range and variety of the self-assembling structures that can be constructed relies on the presence of suitable metal-ligand interactions and supramolecular contacts, as well as the solvents employed. These new complexes thus prepared have attracted a great attention not only due to their intriguing topological features but also their potential applications. The use of Cu(I) ions in the preparation of coordination polymers reflects their application in the area of luminescence that is associated with Cu(I)---Cu(I) interactions (cuprophilicity).[2] It has been reported that the temperature-dependent variation of Cu---Cu distances is responsible for the luminescence thermochromism of the Cu_4I_4 coordination polymers[2a] and the luminescence of 2D Cu(4-pt) [4-pt = 5-(4-pyridyl)tetrazole] coordination polymers can be modified by grinding, which indicates that the mechanochromic properties are related to cuprophilicity and π-π interactions.[2b] Both of the metal ions and the organic spacer ligands provide the opportunities to induce the luminescence, which is also closely related to the guest molecules[2c] and the behavior of hydrogen bonding in the excited state.[2d] Crystal-to-crystal transformations involving coordination polymers are rare due to the involvement of breaking and forming of bonds in more than one direction,[3] and even less common are those that are accompanied by the luminescence change. To our best knowledge, the supramolecular isomerism system of formamidinate ligand-based Cu(I) coordination polymers showing crystal-to-crystal transformations associated with luminescence changes remains unexploited.

The coordination chemistry of metal complexes containing formamidinate ligands has been investigated extensively.[4-6] The copper(II) linear trinuclear compounds of the general formula $[Cu_3(L)_4](CF_3SO_3)_2(Y)_x$ [L is the dehydronated ligands of *N,N'*-bis(pyridine-2-yl)formamidine, *N,N'*-bis(pyrimidine-2-yl)formamidine and *N,N'*-bis(methylpyridine-2-yl)formamidine; Y = EtOH or H_2O and x = 0.5 – 1.5] have been synthesized *in-situ* by the reactions of $Cu(CF_3SO_3)_2$ and triethylorthoformate with 2-aminopyridine, 2-aminopyrimidine and 2-amino-5-methylpyridine,

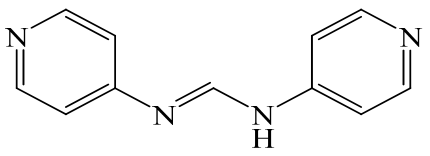

4-Hpyf

respectively, in ethanol at about 40 °C.[5c,d] Apparently, this type of formamidinate ligands could be improved by having different directions of donor sites to construct coordination polymers with higher dimensionality. We report herein the one-pot solvothermal synthesis, structures, crystal-to-crystal transformations and luminescent properties of several 2D and 3D Cu(I) coordination networks based on a formamidinate ligand. A striking feature is that the configurations of the dicopper(I) units of these complexes have a great influence on the luminescent properties. While all of the 2D and 3D *syn*-complexes show broad emissions, those of the 2D *anti*-complexes are not detectable, indicating that the cuprophilicity is unlikely to play significant roles in determining the emissions. The important intermediate **2c** provides a unique evidence that verifies the temperature-dependent crystal-to-crystal transformation upon solvent removal. The adsorption of $CdCl_2$ by the 2D complexes are also investigated.

Experimental sections

General Procedures

Elemental analyses were obtained from a HERAEUS VaruoEL analyzer. IR spectra (KBr disk) were recorded on a Jasco FT/IR-460 plus spectrometer. Thermal gravimetric analyses (TGA) measurements were carried on a TG/DTA 6200 analyzer and the samples were heated up in N_2 with a heating rate of 10 °C min^{-1}. Emission spectra were obtained from a Hitachi F-4500 spectrometer. Powder X-ray diffraction measurements were carried out on a PANalytical PW3040/60 X'Pert Pro diffractometer or on a Bruker D2 PHASER X-ray Diffractometer. SEM/EDS experiments were carried on a JEOL JSM-7600F/Oxford Xmax80 spectrometer. The ^{113}Cd MAS NMR experiments were carried out on a wide-bore 14.1-T Bruker Avance III spectrometer equipped with a 3.2 mm MAS probehead.

Materials

The reagents 4-aminopyridine was purchased from Alfa Aesar, copper(II) acetate from SHOWA, copper(II) tetrafluoroborate, and triethyl orthoformate from Sigma-Aldrich Co. and copper(II) perchlorate from Alfa Aesar. *Caution: Perchlorate salts are dangerous (especially if they are dry) and should be handled with care.*

Synthesis of *anti*-{[Cu(4-pyf)]·ACT}$_n$, 1a, *anti*-{[Cu(4-pyf)]·DMF}$_n$, 1b and *anti*-{[Cu(4-pyf)]·THF}$_n$, 1c

A mixture of $Cu(O_2CCH_3)_2$ (0.18 g, 1.0 mmol), 4-aminopyridine (0.75 g, 8.0 mmol), triethylorthoformate (3.0 mL, 18 mmol) and 5 mL ACT, **1a**, 5 mL DMF, **1b**, or 5 mL THF, **1c**, were placed in a 23 mL Teflon lined stainless container, which was sealed and heated at 120 °C for 48 h under autogenous pressure and then cooled slowly to room temperature. Yellow block crystals were collected, washed by diethyl ether, and dried under vacuum. **1a**: Yield: 0.19 g (56 %). Anal. Calcd. for $C_{14}H_{15}CuN_4O$ (MW = 318.84): C, 52.74; H, 4.74; N, 17.57. Found: C, 52.38; H, 5.25; N, 17.50. IR (KBr disk, cm^{-1}): 3039(w), 1712(w), 1647(w), 1593(w), 1534(m), 1487(m), 1422(w), 1339(m), 1259(w), 1211(w), 1006(w), 966(w), 822(w), 540(w), 420(w), 406(w). **1b**: Yield: 0.27 g (81 %). Anal. Calcd. for $C_{14}H_{16}CuN_5O$ (MW = 333.86): C, 50.21; H, 5.12; N, 20.91. Found: C, 50.18; H, 5.03; N, 19.94. IR (KBr disk, cm^{-1}): 2358(w), 1671(m), 1592(m), 1521(m), 1484(m), 1435(m), 1321(m), 1250(m), 1210(m), 1095(w), 1004(m), 990(m), 825(m), 658(w), 544(w), 410(w). **1c**: Yield: 0.21 g (64 %). Anal. Calcd. for $C_{15}H_{17}CuN_4O$ (MW = 332.87): C, 53.96; H, 5.43; N, 16.78. Found: C, 53.74; H, 5.46; N, 16.36. IR (KBr disk, cm^{-1}): 3433(w), 1592(m), 1526(m), 1479(m), 1340(m), 1247(m), 1208(m), 1004(m), 961(w), 822(m), 729(w), 645(w), 538(w).

Synthesis of *syn*-{[Cu$_4$(4-pyf)$_4$]·2MeOH}$_n$, 2a, *syn*-{[Cu$_4$(4-pyf)$_4$]·2EtOH}$_n$, 2b

Prepared as described for **1a** – **1c** except that MeOH for **2a** and EtOH for **2b** were used as solvents and orange block crystals were collected. **2a**: Yield: 0.21 g (75 %). Anal. Calcd. for $C_{46}H_{44}Cu_4N_{16}O_2$ (MW = 1107.13): C, 49.90; H, 4.01; N, 20.24. Found: C, 50.47; H, 4.21; N, 19.82. IR (KBr disk, cm^{-1}): 3353(m), 3208(m), 2359(w), 1653(m), 1631(m), 1593(m), 1524(s), 1480(s), 1343(s), 1248(m), 1208(s), 1056(w), 1022(m), 1004(m), 960(w), 824(m), 669(w), 646(w), 569(w), 538(m), 472(w), 418(w). **2b**: Yield: 0.20 g (71 %). Anal. Calcd. for $C_{48}H_{48}Cu_4N_{16}O_2$ (MW = 1135.18): C, 49.90; H, 4.01; N, 20.24. Found: C, 50.36; H, 3.87; N, 20.19. IR (KBr disk, cm^{-1}): 3356(w), 3037(w), 2358(w), 1592(m), 1533(s), 1482(s), 1432(w), 1347(s), 1249(m), 1208(s), 1058(w), 1005(m), 992(m), 971(w), 821(m), 734(w), 669(w), 649(w), 541(w), 472(w), 418(w), 403.1(w).

Synthesis of *syn*-{[Cu$_3$(4-pyf)$_2$](BF$_4$)·2H$_2$O·EtOH}$_n$, 3a, and *syn*-{[Cu$_3$(4-pyf)$_2$](ClO$_4$)·EtOH}$_n$, 3b

A mixture of $Cu(O_2CCH_3)_2$ (0.36 g, 2.0 mmol), 4-aminopyridine (0.38 g, 4.0 mmol) and triethylorthoformate (3.0 mL, 18 mmol) in 5.0 mL CH_3CH_2OH were placed in a 23 mL Teflon lined stainless container, followed by addition of $Cu(BF_4)_2$ (0.47 g, 2.0 mmol) for **3a** or $Cu(ClO_4)_2$ (0.74 g, 2.0 mmol) for **3b**. The container was sealed and heated at 120 °C for 48 h under autogenous pressure and then cooled slowly to room temperature. Red block crystals were collected, washed by diethyl ether, and dried under a vacuum. **3a**: Yield: 0.32 g (64 %). Anal. Calcd. for $C_{24}H_{28}BF_4Cu_3N_8O_3$ (MW = 753.97): C, 38.23; H, 3.74; N, 14.86. Found: C, 38.17; H, 3.64; N, 14.60. IR (KBr disk, cm^{-1}): 3398(w), 1652(w), 1602(m), 1537(s), 1485(s), 1348(s), 1254(m), 1208(s), 1084(m), 1053(m), 1031(m), 824(m), 680(w), 545(w). **3b**: Yield: 0.40 g (83 %). Anal. Calcd. for $C_{24}H_{24}Cu_3N_8O_4$ (MW = 730.58): C, 39.46; H, 3.31; N, 15.34. Found: C, 39.87; H, 3.48; N, 15.42. IR (KBr disk, cm^{-1}): 3312(w), 2359(w), 1602(m), 1535(s), 1484(s), 1346(s), 1254(m), 1207(s), 1086(m), 1031(w), 1006(w), 825(m), 623(w), 544(w).

X-ray Crystallography

The diffraction data were collected on a Bruker AXS SMART APEX II diffractometer equipped with a graphite-monochromated MoK_α (λ_α = 0.71073 Å) radiation at 295K (**1a**, **1b**, **1c**, **2a**, **2c**, **3a** and **3b**) or 100 K (compounds **2b**, **2d** and **2e**). Data reduction was carried out by standard methods with use of well-established computational procedures.[7] The structure factors were obtained after Lorentz and polarization correction. An empirical absorption correction based on "multi-scan" was applied to the data. The positions of some of the heavier atoms, including the copper atoms, were located by the direct method. The remaining atoms were found in a series of alternating difference Fourier maps and least-square refinements.[8] All the hydrogen atoms were added by using the HADD command in SHELXTL 5.10 and refined as riding atoms. Basic information pertaining to crystal parameters and structure refinement for **1a**, **1b**, **1c**, **2a**, **2b**, **2c**, **3a** and **3b** is summarized in Table 1 and that for **2d** and **2e** is shown in Table S1. Selected bond distances and angles are listed in Table S2 - Table S4.

Table 1. Crystallographic Data for Compounds **1a - 3b.**

	1a	**1b**	**1c**	**2a**	**2b**	**2c**	**3a**	**3b**
formula	$C_{14}H_{15}CuN_4O$	$C_{14}H_{16}CuN_5O$	$C_{15}H_{17}CuN_4O$	$C_{46}H_{44}Cu_4N_{16}O_2$	$C_{48}H_{48}Cu_4N_{16}O_2$	$C_{52}H_{52}Cu_4N_{16}O_2$	$C_{24}H_{28}BCu_3F_4N_8O_3$	$C_{24}H_{24}ClCu_3N_8O_5$
fw	318.84	333.86	332.87	1107.13	1135.18	1187.26	753.97	730.58
temperature/K	296(2)	296(2)	296(2)	296(2)	100(2)	296(2)	296(2)	296(2)
space group	$P2_1/c$	$P2_1/c$	$P2_1/c$	$C2/c$	$C2/c$	$C2/c$	$P2_1/c$	$P2_1/c$
a, Å	10.6688(3)	9.4249(2)	10.5252(2)	20.8634(7)	20.8705(3)	21.0123(5)	16.2527(9)	16.2717(2)
b, Å	11.4952(3)	14.2699(4)	11.1791(2)	21.3369(8)	21.3742(3)	21.4061(5)	12.3588(8)	12.6684(2)
c, Å	12.9734(3)	11.4988(3)	13.0198(2)	22.7994(8)	22.7059(3)	22.6642(5)	17.4471(10)	17.6021(2)
β, deg	106.7220(10)	100.7050(10)	106.2320(10)	98.646(2)	99.1820(10)	99.4950(10)	114.657(3)	112.5230(10)
V, Å^3	1523.77(7)	1519.59(7)	1470.87(4)	10034.0(6)	9999.1(2)	10054.5(4)	3185.0(3)	3351.68(8)
Z	4	4	4	8	8	8	4	4
D_{calc}, g/cm^3	1.390	1.459	1.503	1.466	1.508	1.569	1.572	1.448
μ, mm^{-1}	1.434	1.443	1.489	1.727	1.735	1.729	2.047	2.008
$2\theta_{max}$, deg	56.50	56.64	56.58	56.62	56.58	52.00	52.00	56.66
no. of reflns meased	13493	14033	13271	49171	59119	42360	26573	32180
no. of reflns used (R_{int})	3752, 0.0279	3757, 0.0218	3628, 0.0285	12385, 0.0628	12388, 0.0430	9872, 0.0520	6255, 0.0598	8300, 0.0270
data completeness (%)	99.5	99.1	99.4	99.2	99.8	100.0	100.0	99.3
no. of params	181	190	190	640	661	614	410	417
GOF on F^2	1.035	1.077	1.054	1.031	1.039	1.073	1.044	1.050
$R_1{}^a$	0.0327	0.0341	0.0281	0.0595	0.0414	0.0578	0.0629	0.0457
$wR_2{}^b$, final R [$I>2\sigma(I)$]	0.0843	0.0973	0.0723	0.1588	0.1065	0.1527	0.1825	0.1423
$R_1{}^a$	0.0458	0.0404	0.0339	0.1056	0.0641	0.0904	0.1028	0.0641
$wR_2{}^b$ (all data)	0.0913	0.1021	0.0757	0.1776	0.1176	0.1706	0.2090	0.1562

[a]$R_1 = \Sigma||F_o| - |F_c|| / \Sigma|F_o|$. [b]$wR_2 = [\Sigma w(F_o^2 - F_c^2)^2 / \Sigma w(F_o^2)^2]^{1/2}$. $w = 1 / [\sigma^2(F_o^2) + (ap)^2 + (bp)]$, $p = [\max(F_o^2 \text{ or } 0) + 2(F_c^2)] / 3$. a = 0.0455, b = 0.5802, **1a**; a = 0.0536, b = 0.8941, **1b**; a = 0.0387, b = 0.8250, **1c**; a = 0.0948, b = 0.0000, **2a**; a = 0.0574, b = 24.0508, **2b**; a = 0.0771, b = 70.9257, **2c**; a = 0.1183, b = 6.1750, **3a**; a = 0.0975, b = 1.2841, **3b**.

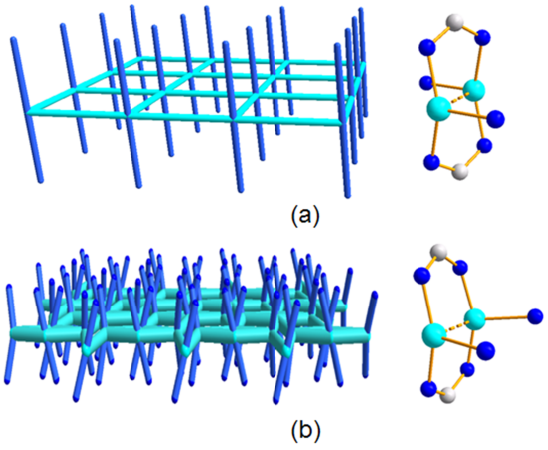

Fig. 1. (a) A representative drawing for **1a** - **1c** with the outward dangling pyridyl nitrogen atoms (left), and a drawing defining the *anti*-configuration (right). (b) A representative drawing for **2a** - **2c** with the outward dangling pyridyl nitrogen atoms (left) and a drawing defining the *syn*-configuration (right).

Adsorption of $CdCl_2$

Adsorption of $CdCl_2$ on **1a** and **2a** were studied at by stirring 0.50 mmol (0.092 g), 1.0 mmol (0.18 g), 1.5 mmol (0.27 g) or 2.0 mmol (0.37 g) of $CdCl_2$ in a solution containing 1.0 mmol (0.32 g) of **1a** in 20 mL ACT or 1.0 mmol (0.28 g) of **2a** in 20 mL MeOH at RT. After 2 hours, the solid was filtered, washed by 100 mL (50 mL x 2) ACT or MeOH and the dried under vacuum. The products were then weighted and the amount of adsorbed $CdCl_2$ calculated and verified by using SEM-EDS and elemental analysis.

Scanning electron microscopy (SEM)

The scanning electron microscopy (SEM) images were prepared by following method: Each sectioned pieces was mounted on copper plate replicas, and the surface was coated with a thin conductive gold layer *via* sputter technique. The SEM image magnifications of all complexes are from 1500 to 40000 with a tilt angle of 0^o and 30^o and the accelerated voltage was operated at 5 kV. The overview of the general surface morphology was obtained by scanning the complexes entirety under low magnification. The detail surface SEM images are from the selected representative area of each complex.

Results and Discussion

Syntheses

One-pot solvothermal reactions of 4-aminopyridine and triethylorthoformate with $Cu(O_2CCH_3)_2$ in acetone (ACT), dimethylformamide (DMF), tetrahydrofuran (THF), methanol (MeOH) and ethanol (EtOH) afforded 2D coordination networks *anti*-$\{[Cu(4\text{-pyf})]\cdot ACT\}_n$, **1a**, *anti*-$\{[Cu(4\text{-pyf})]\cdot DMF\}_n$, **1b**, *anti*-$\{[Cu(4\text{-pyf})]\cdot THF]\}_n$, **1c**, *syn*-$\{[Cu_4(4\text{-pyf})_4]\cdot 2MeOH\}_n$, **2a**, and *syn*- $\{[Cu_4(4\text{-pyf})_4]\cdot 2EtOH\}_n$, **2b**, whereas the reaction of $Cu(O_2CCH_3)_2$, 4-aminopyridine, triethylorthoformate and CuX_2 (X = BF_4^- and ClO_4^-) in ethanol gave the 3D coordination networks *syn*-$\{[Cu_3(4\text{-pyf})_2](BF_4)\cdot 2H_2O\cdot EtOH\}_n$, **3a** and *syn*-$\{[Cu_3(4\text{-pyf})_2](ClO_4)\cdot EtOH\}_n$, **3b**, respectively. Several different molar ratios of $Cu(O_2CCH_3)_2$: 4-aminopyridine : triethylorthoformate have been used to grow crystals under solvothermal conditions for complexes **1a** – **3b**. The molar ratio that gave the highest yield is 1 : 8 : 18 for

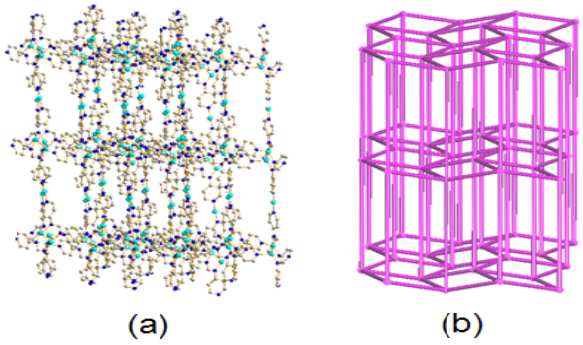

Fig. 2. (a) A representative drawing showing the 3D structures of **3a** and **3b**. (b) A simplified 3D structure for **3a** and **3b** with the **pcu** topology.

complexes **1a** – **2b**, whereas the ratio of $Cu(O_2CCH_3)_2$: 4-aminopyridine : triethylorthoformate : CuX_2 (X = BF_4 or ClO_4) that gave the highest yield is 1: 2: 9 : 1 for complexes **3a** and **3b**. The crystals of **3a** and **3b** can not be obtained if $Cu(O_2CCH_3)_2$ are replaced by the same equivalents of $Cu(BF_4)_2$ or $Cu(ClO_4)_2$ and only in MeOH and EtOH can they be prepared. It is noted that excess amount of triethylorthoformate was used to give better yields. All compounds formed as phase-pure yellow plates (**1a** – **1c**) and red plates (**2a**, **2b**, **3a** and **3b**), respectively. Attempts to prepare **3a** and **3b** by the reactions of the **1a** – **2b** with $Cu(BF_4)_2$ or $Cu(ClO_4)_2$ under reflux or solvothermal conditions led to the decomposition of the 2D coordination networks. The formation of these complexes show two features involving the one-pot polymerization and reduction of Cu(II) to Cu(I). The reduction process has been frequently observed for hydro(solvo)thermal conditions with amine or pyridine containing ligands such as 4,4'-bipyridine that may serve as effective reducing agent for Cu(II) to Cu(I).[9] It is noted that all these complexes are insoluble in most of the common solvents, especially in the solvents mentioned above.

Structures of 1a – 1c

The structures of **1a** – **1c** were solved in the space group $P2_1/c$. Fig. S1(a) depicts a representative drawing showing the coordination environments about Cu(I) ions. The two Cu(I) ions that are bridged by two 4-pyf ligands through two central amine nitrogen atoms and coordinated by the pyridyl nitrogen atoms from adjacent dicopper units adopt the distorted T-shaped geometries with the Cu(I)---Cu(I) distances of 2.5444(5), 2.5471(5) and 2.5348(3) Å for **1a** – **1c**, respectively, resulting in 2D planar layers, Fig. S1(b). The planar layers can be simplified as the 4-connected nets with the $\{4^4\cdot 6^2\}$-**sql** topology determined using TOPOS.[10] Each of the 4-pyf ligands adopts the κ^3-bonding mode with one dangling pyridyl nitrogen atom. Fig. 1(a) depicts a simplified schematic drawing for the 2D planar layer with the outwardly dangling nitrogen atoms. The N-Cu-Cu-N dihedral angles involving the two pyridyl nitrogen atoms that are coordinated to the Cu(I) ions are all 180^o, and are designated as the *anti*-configuration. Noticeably, short interlayer π-π distances of 3.90 and 3.97 Å between the 2D layers are found for **1a** and **1c**, respectively, resulting in cavities that encapsulate the solvents, Fig. S1(c). Fig. S1(d) depicts a simplified supramolecular 3D structure for **1a** and **1c**, showing the cavities occupied by the solvents and the **pcu** topology. It is noted that the π-π distance is 4.48 Å for **1b** and the typical cutoff distance for π - π stacking interactions is 3.9 Å.[11]

Structures of 2a – 2c

The structures of **2a** – **2c** were solved in the space group *C*2/*c*. Fig. S2(a) depicts a representative drawing showing the coordination environments about the Cu(I) ions. The core structures of the dicopper units are similar to those of **1a** – **1c**, in which pairs of Cu(I) ions are bridged by two 4-pyf` ligands and coordinated by the pyridyl nitrogen atoms, leaving one dangling pyridyl nitrogen atom for each of the 4-pyf` ligands and resulting in 2D pleated layers, Fig. S2(b). The Cu(I) ions show T-shaped coordination environments with the Cu(I)---Cu(I) distances in the range 2.4968(13) - 2.5463(12) Å. In marked contrast to **1a** – **1c**, the N-Cu-Cu-N dihedral angles of **2a** – **2c** involving the two pyridyl nitrogen atoms that are coordinated to the Cu(I) ions are 0.23 - 8.78°, which are less than 90° and are designated as the *syn*-configurations. Fig. 1(b) depicts a schematic drawing for the 2D pleated layer and the outwardly dangling pyridyl nitrogen atoms. The 2D pleated layers of **2a** – **2c** can also be simplified as the 4-connected net with the $\{4^4\cdot6^2\}$-**sql** topology, Fig. S2(c). Short intralayer π-π distances in the range 3.49 – 3.76 Å are also observed in the 2D layers of **2a** – **2c**. and **2b**, which increases the vibration modes and thus reduces the time for vibrational relaxation.

Structures of 3a and 3b

The structures of **3a** and **3b** were solved in the space group $P2_1/c$. Fig. S3 depicts a representative drawing showing the coordination environments about Cu(I) ions. The Cu(I) ions show T-shaped coordination environments with the Cu(I)---Cu(I) distances of 2.5540(9) and 2.5716(4) Å for **3a** and **3b**, respectively. The N-Cu-Cu-N dihedral angles involving two pyridyl nitrogen atoms are 1.17° for **3a** and 4.02° **3b**, respectively, showing the *syn*-configurations as complexes **2a** – **2c**. The striking feature is that dangling pyridyl nitrogen atoms in **2a** and **2b** are now coordinated by the Cu(I) ions, resulting in 3D coordination networks, with Cu(3)-N distances of 1.873(8) - 1.938(16) Å for **3a** and 1.876(2) - 1.888(3) Å for **3b**, respectively. The 3D structures can be simplified as the 6-connected nodal nets with the $\{4^{12}\cdot6^3\}$-**pcu** topology, Fig. 2. Short π-π distances of 4.00 and 3.98 Å are also observed in **3a** and **3b**, respectively.

The Cu---Cu distances of **1a** – **3b**, 2.5027(5) – 2.5716(4) Å, are shorter than the sum of the Van der Waals radii of Cu(I) centers (2.8 Å), indicating the existence of "cuprophilicity". It is also noted that in the dicopper units of **1a** – **3b**, the Cu-N distances to the inner nitrogen atoms that are 1.927(5) - 1.978(2) Å are significantly shorter than those to the pyridyl nitrogen atoms, which are 2.075(4) - 2.191(4) Å.

Thermal Properties

Thermal gravimetric analyses (TGA) and differential scanning calorimetry (DSC) were carried out to examine the thermal stabilities of complexes **1a** – **2b**. The TGA curves of complexes **1a** – **2b**, Fig. S4(a) and Table S5, involve two major weight losses. The first weight losses in the range 60 - 220 °C are due to the removal of the solvent molecules, whereas the second weight losses in 280 - 800 °C can be ascribed to the decomposition of the 4-pyf` ligands. The DSC curves, Fig. S4(b) and Fig. S4(c) and Table S6, show exothermic peaks at 81, 73 and 81 °C for **1a - 1c**, respectively, which can be ascribed to the *anti* to *syn* transformation in which the solvent molecules are retained, *vide infra*. The large endothermic peaks at 153, 179 and 155 °C are due to the removal of the solvent molecules. The DSC curves show stepwise solvent losses with endothermic peaks at 86 and 172 °C for **2a** and 75 and 143 °C for **2b**, respectively. The small exothermic peaks at 201, 199, 196, 202 and 203 °C for **1a** – **2b**, respectively, are due to the phase transition of the desolvated **1a** – **2b**. The DSC curves show endothermic peaks at 105 °C for **3a**

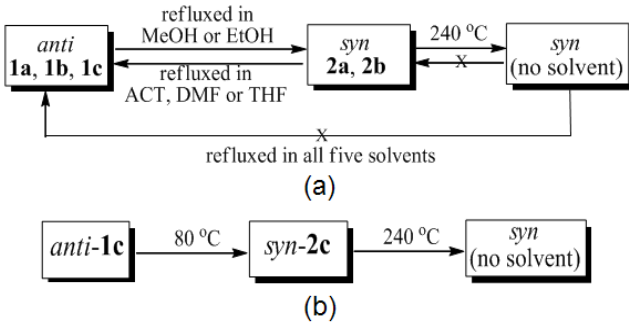

Fig. 3. (a) Reversible and irreversible crystal-to-crystal transformations among *syn* and *anti* complexes. (b) Crystal-to-crystal transformations between **1c** and **2c**.

and 135 °C for **3b**, which are due to removal of the solvent molecules, Fig. S4(c).

Crystal-to-Crystal transformation

Reversible *syn* ⇌ *anti* transformations due to solvent exchange

Complexes **1a** – **2b** provide an opportunity to investigate the structural transformations due to solvent exchange and solvent removal in the Cu(I) coordination networks containing the formamidinate ligands. To confirm the transformations in **1a** – **2b**, we first checked their purities by measuring the powder X-ray diffraction patterns. Fig. S5 – Fig. S9 show that the powder patterns of these five complexes match quite well with those simulated from single-crystal X-ray data, indicating the bulk purities of these complexes. We then investigated the solvent-exchange reactions of these 2D coordination networks. We first heated 0.10 g of **1a**, **1b** or **1c** in 10 mL MeOH or EtOH to reflux for 30 minutes. The insoluble crystalline solids were then collected and then dried under vacuum. By using the PXRD patterns, as shown in Fig. S10 – Fig. S21, we found that these complexes have been transformed to **2a** or **2b**. Similarly, by heating **2a** or **2b** in ACT, DMF and THF to reflux for 30 minutes, complexes **1a**, **1b** and **1c** can be obtained, respectively, indicating the reversible *syn* ⇌ *anti* structural transformations due to the solvent exchange at refluxing temperatures. The *syn* ⇌ *anti* isomerization should involve the breaking of the Cu-N bonds to the pyridyl nitrogen atoms and the coordination of the dangling pyridyl nitrogen atoms to the Cu(I) ions.

Irreversible *anti* to *syn* transformation due to solvent removal

To investigate the structural transformation upon solvent removal, we have heated the crystals of **1a** – **2b** at 240 °C to remove the solvents. It is noted that removal of the solvent molecules from **1a** – **1c** under vacuum at room temperature is not possible, probably due to the encapsulation of the solvent molecules in the structures, *vide supra*. Fortunately, we were able to obtain two types of crystals suitable for X-ray diffraction measurements by heating **2b** at 140 °C and 180 °C, which conform to the space groups *I*-4, **2d**, and *I*-4c2, **2e**, respectively, Table S1. Analysis of the powder X-ray diffraction patterns of the desolvated products of **1a - 2b** at 240 °C shows that the major components of each of these desolvated products is a mixture of **2d** and **2e** with a ratio of about 1 : 1, Fig. S22 – Fig. S23. Although the qualities of the crystals of **2d** and **2e** are poor, their structures clearly indicate the formation of 2D layers with the dicopper units adopting the *syn*-configuration. Most interestingly, we were able to obtain single crystals of *syn*-$\{[Cu_4(4\text{-pyf})_4]\cdot2THF\}_n$, **2c**, by heating **1c** at 80 °C for 30 minutes. Structural determination using single-crystal crystallography revealed that **2c** adopts the *syn*

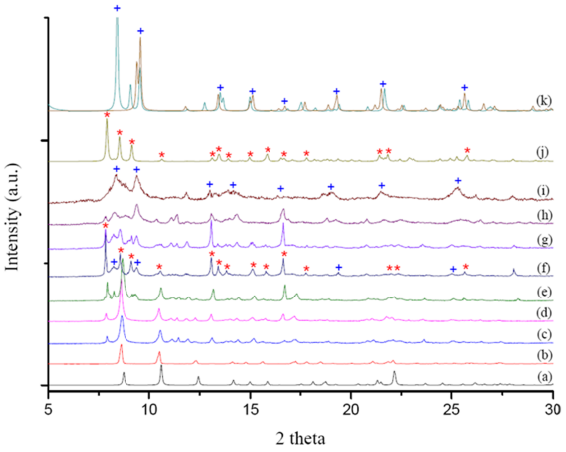

Fig. 4. (a) Simulated PXRD patterns for **1c** and patterns at (b) 30, (c) 50, (d) 60, (e) 80, (f) 85, (g) 100, (h) 140 and (i) 160 °C. (j) Simulated pattern for **2c**. (k) Combined simulated patterns for **2d** and **2e**.

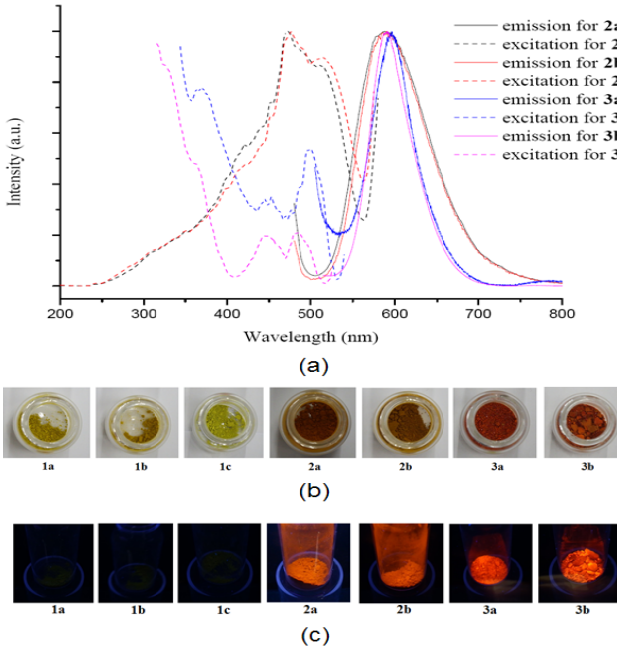

Fig. 5. (a) Emission and excitation spectra of complexes **2a**, **2b, 3a** and **3b** in the solid state at room temperature. (b) Images of complexes **1a** - **3b**. (c) Images showing emissions of **1a** - **3b** upon excitation at 365 nm.

configuration with the cocrystallized THF solvents. The whole processes from the *anti*-complexes **1a** – **1c** to the desolvated **2d** and **2e** are thus most probably temperature-dependent. Fig. 3 shows all the possible pathways for the crystal-to-crystal transformations. To further confirm this temperature-dependent transformation, we measured the variable temperature PXRD patterns for **1c**, Fig. 4. The X-ray powder patterns at 85 °C show a mixture of **2c** (denoted by the red star sign) and the desolvated product (denoted by the blue plus sign). The peaks noted by the red stars match quite well with those in the simulated pattern of **2c**. The intensities of the peaks of **2c** decrease and those of the desolvated product increase as the temperature increases. It is noted that refluxing the desolvated

Table 2. Solid-state absorption and luminescence data for complexes **1a** - **3b** at room temperature.

Complex	Absorption	Emission		Lifetime
	λ_{abs}, nm	λ_{em}, nm	λ_{ex}, nm	τ, ns
1a	430	no emission		
1b	454	no emission		
1c	446	no emission		
2a	498	588	472	27.22
2b	493	590	476	21.52
3a	330, 451, 512	603	499	2.26
3b	355, 482, 539	598	485	3.38
Desolvated 1a		574	502	
Desolvated 1b		576	501	
Desolvated 1c		570	500	
Desolvated 2a		576	499	
Desolvated 2b		575	502	

products of **1a** – **2b** in various solvents did not lead to the formation of the original compounds, indicating that *anti*-to-*syn* transformations upon solvent removal are irreversible. The structures of **3a** and **3b** remain stable upon solvent removal, Fig. S24 – Fig. S25.

Absorption and emission properties

Fig. S26(a) show the solid-state UV-vis spectra of **1a** – **3b** that display lowest energy bands in the range 430 – 539 nm. The emission spectra of the ground samples of **1a** – **3b** were measured in the solid state at room temperature, Fig. 5(a) and Table 2. The crystalline samples gave the similar emission results as the ground samples, Fig. S26(b) and Table S7. Interestingly, only the *syn*-complexes, **2a**, **2b**, **3a** and **3b** and the desolvated products of **1a** – **3b** show broad emission bands, Fig. S27, whereas no detectable levels of emission intensity can be found for the *anti*-complexes **1a** - **1c**, Fig. 5(c). The undetectable emission intensity for **1a** - **1c** may be due to the non-radiative decay[12] of the absorbed light by the *anti* complexes in the solid state, indicating that the emissions are configurationally controlled and the cuprophilicity is unlikely to play significant roles in determining the emissions of **1a** – **3b**. It is also noted that the π-π distances of the 2D *syn*-complexes, **2a** and **2b** (3.49 – 3.76 Å) are significantly shorter than those of the 2D *anti*-complexes **1a** - **1c** (3.89, 4.48 and 3.96 Å), probably indicating that undetectable emission for **1a** - **1c** is due to the longer π-π stacking interactions resulting from the *anti*-configuration.[13] The facts that the lifetimes of the emissions are in the nanosecond range (27.22 ns for **2a**, 21.52 ns for **2b**, 2.26 ns for **3a** and 3.38 ns for **3b**) and the absorption and emission bands show small separations (stock shifts) of 3074 cm^{-1} for **2a**, 3335 cm^{-1} for **2b**, 2948 cm^{-1} for **3a** and 1830 cm^{-1} for **3b**, respectively, suggest that the emissions are probable fluorescence. The smaller lifetimes for **3a** and **3b** may be ascribed to the coordination of the Cu(I) ions to the dangling nitrogen atoms of **2a** and **2b**, which increases the vibration modes and thus reduces the time for vibrational relaxation.

In order to get more insight into electronic and luminescent properties of these complexes, a time-dependent density functional theory (TD-DFT)[14] was performed on the *syn*- and *anti*-complexes at the B3LYP/6-311++G(d,p) level,[15] which is implemented by the Gaussian 09W software package.[16] The coordinates of the asymmetric units for **1b** and **2b** from single crystal crystallography were used to define the *syn*-and *anti*-coordination networks in

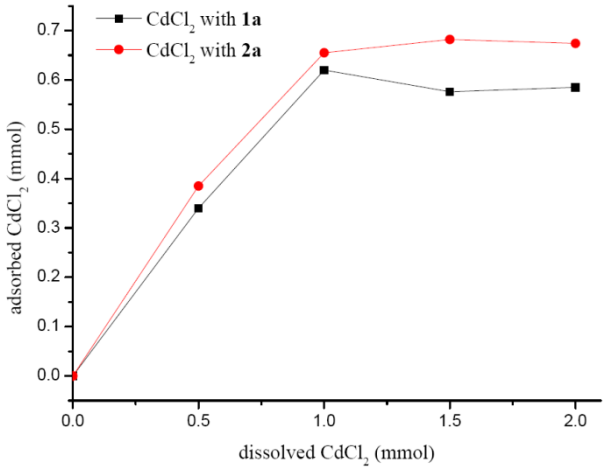

Fig. 6. Adsorption isotherms for $CdCl_2$ by **1a** and **2a**

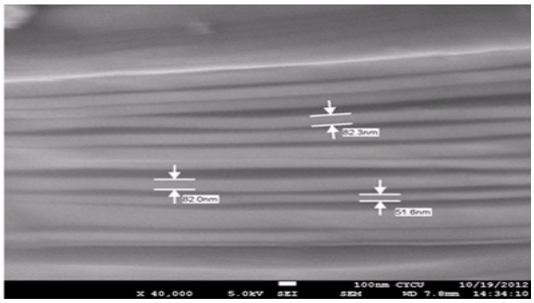

(a)

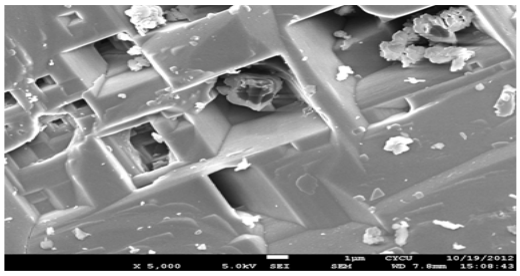

(b)

Fig. 7. (a) SEM image for crystalline **2b** at RT, scal bar is 100 nm. (b) SEM image for crystalline **2b** after heated at 180 °C, scal bar is 1 μm.

Cartesian coordinate system, assuming C_i (*gerade* symmetry) and C_2 (*ungerade* symmetry) point groups with Cu-Cu vector along the *z* axis. The ligands that link the $Cu_2(4\text{-pyf})_2$ units were reduced as pyridine molecules. The results show that the HOMOs of both the *syn* and *anti* complexes are mainly composed of d orbitals (61.06 % for *syn* and 63.26 % for *anti*) of the Cu(I) ions and the LUMOs are mainly composed of π*-orbitals from the ligand, with the HOMO-LUMO separations of 2.61 eV for *syn* complex and 3.23 eV for *anti* complex, respectively, Table S8 and Fig. S28. The lowest energy bands of **1a** – **3b** in the solid state UV-vis spectra can thus most probably be assigned to the 3dσ*/δ*→pπ* transitions,[2g,2h] which are also responsible for the emission bands of **2a** – **3b**.

$CdCl_2$ adsorption

Complexes **1a** – **2b** show 2D layers with outwardly dangling pyridyl nitrogen atoms. The adsorptions of $CdCl_2$ by **1a** and **2a** were thus investigated by using SEM-EDS and elementary analysis, Fig. S29 and Fig. S30 and Tables S9 and S10. Adsorption isotherms, Fig. 6, at different molarities of dissolved $CdCl_2$ show that the number of mole of adsorbed $CdCl_2$ increases as the concentration of the dissolved $CdCl_2$ increases, which may reach the maximum adsorption at about 1.0 mmol of the dissolved $CdCl_2$. It is noted that there is only one dangling nitrogen atom per formula of **1a** or **2a** and 1.0 mmol of **1a** or **2a** was used for adsorbing $CdCl_2$. To evaluate the interactions between the adsorbed $CdCl_2$ and the coordination network, we have measured the solid state ^{113}Cd MAS NMR spectra of the adsorbed products, Fig. S31. It has been shown that the reported ^{113}Cd chemical shifts of the compounds coordinated by nitrogen atoms are between 200 – 380 ppm,[17] and the crystalline $CdCl_2$ shows peak at 183.0 ppm.[17a] Because the spectrum of the product obtained by adding $CdCl_2$ to the ACT solution of **1a** shows three board peaks at 126.4, 186.1 and 220.2 ppm, and that of $CdCl_2$ in **2a** shows a board peak at 229.9 ppm, we suggest that most of the adsorbed $CdCl_2$ interact with **1a** and **2a** through the Cd---N interactions to the nitrogen atoms of the dangling pyridyl rings.

Scanning electron microscopy (SEM)

Fig. S32 depicts SEM images of the crystals of **2b** at room temperature, and Fig. 7(a) shows a 40000 magnification image. The structure of the crystals is lamellar with slits between layers and the thickness of the layers are in the range of 51.6 - 82.3 nm. The image of **2b** after heated to 180 °C, Fig. 7(b), shows the disappearance of the slits and the the formation of cubical defects. Inspection of the surfaces of the defects reveals the round cavities, Fig. S33, with diameters near 50 nm. Such huge defects may be responsible for the irreversible transformations of **1a** – **2b** to the desolvated products.

Conclusions

By one-pot solvothermal reactions of 4-aminopyridine and triethylorthoformate with divalent copper salts, several 2D and 3D coordination networks have been prepared, in which the aprotic solvents ACT, DMF and THF and the protic solvents MeOH and EtOH favor the formation of complexes with *anti*- and *syn*-configurations, respectively. The 2D *anti*- and *syn*- coordination networks can be reversibly interconverted through solvent exchanges, resulting from the breaking and making of the Cu-N bond to the pyridyl nitrogen atoms. The characterization of the intermediate **2c** demonstrates that the irreversible *anti*-to-*syn* transformations upon solvent removal are temperature-dependent. The configurations of the structures have significant influences on the emission properties. While the *syn*-complexes show broad emissions, those of the *anti*-complexes are not detectable, indicating that cuprophilicity is unlikely to play significant roles in determining the emissions of **1a** – **3b**. The solvents in the present system are important in determining the structural diversity; however, they are not responsible for the luminescene since the desolvated products are luminescent. We have also shown that the 2D *anti*- and *syn*-complexes that show outwardly dangling pyridyl rings may adsorb the Cd(II) salts through Cd---N interactions

Acknowledgment

We are grateful to the Ministry of Science and Technology of the Republic of China for support.

Notes and reference

[a]Department of Chemistry, Chung Yuan Christian University, No. 200, Chung Pei Road, Chung-Li, 320, Taiwan.

E-mail: jdchen@cycu.edu.tw
[b]Department of Applied Chemistry, National Pingtung University, No. 4-18 Minsheng Road, Ping-Tung, 900, Taiwan.

† Electronic Supplementary Information (ESI) available: Crystallographic data for **2d** and **2e** (Table S1). Selected bond lengths for **1a** – **3b** (Table S2 – S4). TGA analyses for **1a** – **2b**. DSC parameters for **1a** – **3b** (Table S5 and S6). Luminescence data for crystalline **2a** – **3b** (Table S7). Electronic contributions (Table S8). SEM-EDS results of **1a** and **2a** (Table S9 and S10).Coordination environments for **1a** – **3b** (Fig. S1 – Fig. S3). TGA curves for **1a** – **2b** and DSC curves for **1a** – **3b** (Fig. S4). Powder XRD patterns for **1a** – **2b** (Fig. S5 – Fig. S9). Solvent-induced SCSC transformation PXRD patterns for **1a** – **2b** (Fig. S10 – Fig. S21). Temperature-dependent PXRD patterns for **1a** – **2b** (Fig. S22 and Fig. S23). PXRD patterns for **3a** (Fig. S24) and **3b** (Fig. S25). Solid-state UV-vis, emission and excitation spectra for crystalline **2a** – **3b** (Fig. S26). Emission spectra for desolvated **1a** – **2b** (Fig. S27). Energy gaps for *syn*- and *anti* complexes (Fig. S28). SEM-EDS images of **1a** and **2a** (Fig. S29 and Fig. S30). ^{113}Cd solid-state NMR spectra (Fig. S31). SEM images for **2b** at RT (Fig. S31) and after heated at 180 ^{o}C (Fig. S32). CCDC 1017750 - 1017757. For ESI and crystallographic data in CIF or other electronic format see DOI: 10.1039/b000000x/

1 (a) M. O'Keefee and O. M. Yaghi, *Chem. Rev.*, 2012, **112**, 675-702; (b) S. Kitagawa, S. Noro and T. Nakamura, *Chem. Comm.*, 2006, 701-707; (c) S. Kitagawa, R. Kitaura and S. Noro, *Angew. Chem. Int. Ed.*, 2004, **43**, 2334-2375; (d) J.-R. Li, J. Sculley and H.-C. Zhou, *Chem. Rev.*, 2012, **112**, 869-932; (e) H. Furukawa, K. E. Cordova, M. O'Keeffe and O. M. Yaghi, *Science*, 2013, **341**, 123044; (f) T. H. Rark, A. J. Hickman, K. Koh, S. Martin, A. G. Wong-Foy, M. S. Sanford and A. J. Matzger, *J. Am. Chem. Soc.*, 2011, **133**, 20138-20141.

2 (a) T. H. Kim, Y. W. Shin, J. H. Jung, J. S. Kim and J. Kim, *Angew. Chem. Int. Ed.*, 2008, **47**, 685-688; (b) T. Wen, X.-P. Zhou, D.-X. Zhang and D. Li, *Chem. Eur. J.*, 2014, **20**, 644-648; (c) Y. Cui, Y. Yue, G. Qian and B. Chen, *Chem. Rev.*, 2012, **112**, 1126-1162; (d) G. J. Zhao and K. L. Han, *ChemPhysChem*, 2008, **9**, 1842-1846; (e) C.-M. Che, Z. Mao, V. M. Miskowski, M.-C. Tse, C.-K. Chan, K.-K. Cheung, D. L. Phillips and K.-H. Leung, *Angew. Chem. Int. Ed.*, 2000, **39**, 4084-4088; (f) P. Pyykkö, *Chem. Rev.*, 1997, **97**, 597-636; (g) Y. Chen, J.-L. Li, G. S. M. Tong, W. Lu, W. -F. Fu, S.-W. Lai and C.-M. Che, *Chem. Sci.*, 2011, **2**, 1509-1514; (h) V. W.-W. Yam and K. M.-C. Wong, *Chem. Commum.*, 2011, **47**, 11579-11592.

3 (a) J. J. Vittal, *Coord. Chem. Rev.*, 2007, **251**, 1781-1795; (b) G. K. Kole and J. J. Vittal, *Chem. Soc. Rev.*, 2013, **42**, 1755-1775.

4 F. A. Cotton, C. A. Murillo and R. A. Walton, *Multiple Bonds Between Metal Atoms*, 3rd ed., Springer Science and Business Media, Inc., New York, 2005.

5 a) Z.-K. Chan, T.-R. Chen, J.-D. Chen, J.-C. Wang and C.-W. Liu, *Dalton Trans*., 2007, 3450-3458; (b) Z.-K. Chan, C.-H. Lin, C.-C. Wang, J.-D. Chen, J.-C. Wang and C.-W. Liu, *Dalton Trans.*, 2008, 2189-2189; (c) G. A. V. Albada, P. J. V. Koningsbruggen, I. Mutikainen, U. Turpeinen and J. Reedijk, *Eur. J. Inorg. Chem.*, 1999, 2269-2275; (d) G. A. V. Albada, I. Mutikainen, T. Urho and J. Reedijk, *Eur. J. Inorg. Chem.*, 1998, 547-549.

6 W. Hsu, Y.-S. Li, H.-Y. He, K.-T. Chen, H.-S. Wu, D. M. Proserpio, J.-D. Chen and J.-C. Wang, *CrystEngComm*, 2014, **16**, 7385-7388.

7 *Bruker AXS, APEX2, V2008.6; SAD ABS V2008/1; SAINT+ V7.60A; SHELXTL V6.14*; Bruker AXS Inc.: Madison, Wisconsin, USA, 2008.

8 G. M. Sheldrick, *Acta Crystallogr.*, 2008, **A64**, 112-122.

9 (a) J. Y. Lu and A. M. Babb, *Inorg. Chem.*, 2002, **41**, 1339-1341; (b) S. M-F. Lo, S. S-Y. Chui, L.-Y. Shek, Z.-Y. Lin, X.-X, Zhang, G.-H. Wen and I. D. Williams, *J. Am. Chem. Soc.*, 2000, **122**, 6293-6294; (c) K. Jin, X.-Y. Huang, L. Pang, J. Li, A. Appel and S. Wherland, *Chem. Commun.*, 2002, 2872-2873.

10 V. A. Blatov, A. P. Shevchenko and D. M. Proserpio, *Cryst. Growth Des.*, 2014, **14**, 3576-3586. See also: http://www.topos.samsu.ru/

11 K. I. Nattinen and K. Rissanen, *Cryst. Growth Des.*, 2003, **3**, 339-353.

12 N. J. Turro, *Modern Molecular Photochemistry*, University Science Books, California, 1991.

13 (a) T. McCormick, W.-L. Jia and S. Wang, *Inorg. Chem.*, 2006, **45**, 147-155; (b) C.-M. Che and S.-W. Lai, *Coord. Chem. Rev.*, 2005, **249**, 1296-1309.

14 (a) P. Hohenberg and W. Kohn, *Phys. Rev.*, 1964, **136**, B864-B871; (b) R. G. Parr and W. Yang, *Density-Functional Theory of Atoms and Molecules*; Oxford University Press, Oxford, 1989.

15 (a) A. D. Becke, *J. Chem. Phys.*, 1993, **98**, 5648-5652; (b) A. D. Becke, *Phys. Rev. A*, 1988, **38**, 3098-3100; (c) C. T. Lee, W. T. Yang and R. G. Parr, *Phys. Rev. B*, 1988, **37**, 785-789.

16 M. J. Frisch, G. W. Trucks, H. B. Schlegel, G. E. Scuseria, M. A. Robb, J. R. Cheeseman, G. Scalmani, V. Barone, B. Mennucci, G. A. Petersson, H. Nakatsuji, M. Caricato, X. Li, H. P. Hratchian, A. F. Izmaylov, J. Bloino, G. Zheng, J. L. Sonnenberg, M. Hada, M. Ehara, K. Toyota, R. Fukuda, J. Hasegawa, M. Ishida, T. Nakajima, Y. Honda, O. Kitao, H. Nakai, T. Vreven, Jr., J. A. Montgomery, J. E. Peralta, F. Ogliaro, M. Bearpark, J. J. Heyd, E. Brothers, K. N. Kudin, V. N. Staroverov, T. Keith, R. Kobayashi, J. Normand, K. Raghavachari, A. Rendell, J. C. Burant, S. S. Iyengar, J. Tomasi, M. Cossi, N. Rega, J. M. Millam, M. Klene, J. E. Knox, J. B. Cross, V. Bakken, C. Adamo, J. Jaramillo, R. Gomperts, R. E. Stratmann, O. Yazyev, A. J. Austin, R. Cammi, C. Pomelli, J. W. Ochterski, R. L. Martin, K. Morokuma, V. G. Zakrzewski, G. A. Voth, P. Salvador, J. J. Dannenberg, S. Dapprich, A. D. Daniels, O. Farkas, J. B. Foresman, J. V. Ortiz, J. Cioslowski and D. J. Fox, *Gaussian 09*, Revision B.01, Gaussian, Inc., Wallingford CT, 2010.

17 (a) S. Sakida, M. Shojiya and Y. Kawamoto, *Solid State Commun.*, 2000, **115**, 553-588; (b) M. F. Summers, *Coord. Chem. Rev.*, 1988, **86**, 43-134; (c) R. March, J. Pons, J. Ros, W. Clegg, A. Álvarez-Larena, J. F. Piniella and J. Sanz, *Inorg. Chem.*, 2003, **42**, 7403-7409; (d) M. I. M. Wazeer and A. A. Isab, *Spectrochim. Acta, A.*, 2005, **62**, 880-885.